Inorg. Chem. **2009**, *48*, 1753−1762

Organometallic Osmium(II) Arene Anticancer Complexes Containing Picolinate Derivatives

Sabine H. van Rijt,[†] Anna F. A. Peacock,[‡] Russell D. L. Johnstone,[‡] Simon Parsons,[‡] and Peter J. Sadler*,[†]

Department of Chemistry, University of Warwick, Gibbet Hill Road, Coventry CV4 7AL, U.K., and School of Chemistry, University of Edinburgh, West Mains Road, Edinburgh EH9 3JJ, U.K.

Received October 22, 2008

Chlorido osmium(II) arene [(η^6-biphenyl)Os^{II}(X-pico)Cl] complexes containing X = Br (**1**), OH (**2**), and Me (**3**) as *ortho*, or X = Cl (**4**), CO_2H (**5**), and Me (**6**) as *para* substituents on the picolinate (pico) ring have been synthesized and characterized. The X-ray crystal structures of **1** and **6** show typical "piano-stool" geometry with intermolecular π-π stacking of the biphenyl outer rings of **6**. At 288 K the hydrolysis rates follow the order **2** ≫ **6** > **4** > **3** > **5** ≫ **1** with half-lives ranging from minutes to 4.4 h illustrating the influence of both electronic and steric effects of the substituents. The pK_a values of the aqua adducts **3A**, **4A**, **5A**, and **6A** were all in the range of 6.3−6.6. The *para*-substituted pico complexes **4**−**6** readily formed adducts with both 9-ethyl guanine (9EtG) and 9-ethyl adenine (9EtA), but these were less favored for the *ortho*-substituted complexes **1** and **3** showing little reaction with 9EtG and 9EtA, respectively. Density-functional theory calculations confirmed the observed preferences for nucleobase binding for complex **1**. In cytotoxicity assays with A2780, cisplatin-resistant A2780cis human ovarian, A549 human lung, and HCT116 colon cancer cells, only complexes **4** (*p*-Cl) and **6** (*p*-Me) exhibited significant activity (IC_{50} values < 25 μM). Both of these complexes were as active as cisplatin in A2780 (ovarian) and HCT116 (colon) cell lines, and even overcome cisplatin resistance in the A2780cis (ovarian) cell line. The inactivity of **5** is attributed to the negative charge on its *para* carboxylate substituent. These data illustrate how the chemical reactivity and cancer cell cytotoxicity of osmium arene complexes can be controlled and "fine-tuned" by the use of steric and electronic effects of substituents on a chelating ligand to give osmium(II) arene complexes which are as active as cisplatin but have a different mechanism of action.

Introduction

Currently, there is much interest in ruthenium(II) arene complexes of the type [(η^6-arene)Ru(X)(YZ)] (where YZ is a bidentate chelating ligand, and X a good leaving group, e.g. Cl^-) which exhibit both in vitro and in vivo anticancer activity, in some cases even comparable to that of cisplatin.[1] Yet the pharmacological potential of the heavier congener osmium has been little explored. Previous work in our laboratory on Os^{II} arene complexes, [(η^6-arene)Os(YZ)X]$^{n+}$, has shown that their aqueous reactivity is highly dependent on the nature of the chelating ligand YZ.[2,3]

A lack of understanding of the aqueous chemistry of organometallic complexes, in particular of Ru^{II} and Os^{II} arene complexes, under biologically relevant conditions provides an obstacle in current attempts to design anticancer drugs. Knowledge of the aqueous chemistry of these types of complexes may eventually lead to the control of their pharmacological properties, including cell uptake, distribution, DNA binding, metabolism, and toxic side-effects.

For the Os^{II} arene ethylenediamine (en) complex, [(η^6-biphenyl)Os(en)Cl]$^+$, hydrolysis occurs with a half-life of 6.4 h at 298 K, which is about 40 times slower than that

* To whom correspondence should be addressed. E-mail: p.j.sadler@warwick.ac.uk.
† University of Warwick.
‡ University of Edinburgh.

(1) Aird, R. E.; Cummings, J.; Ritchie, A. A.; Muir, M.; Morris, R. E.; Chen, H.; Sadler, P. J.; Jodrell, D. I. *Br. J. Cancer* **2002**, *86*, 1652.
(2) Peacock, A. F. A.; Habtemariam, A.; Fernandez, R.; Walland, V.; Fabbiani, F. P. A.; Parsons, S.; Aird, R. E.; Jodrell, D. I.; Sadler, P. J. *J. Am. Chem. Soc.* **2006**, *128*, 1739.
(3) (a) Peacock, A. F. A.; Parsons, S.; Sadler, P. J. *J. Am. Chem. Soc.* **2007**, *129*, 3348. (b) Krostrhunova, H.; Florian, J.; Novakova, O.; Peacock, A. F. A.; Sadler, P. J.; Brabec, V. *J. Med. Chem.* **2008**, *51*, 3635.

10.1021/ic8020222 CCC: $40.75
Published on Web 01/15/2009

Chart 1. Osmium Arene Complexes Studied in This Work

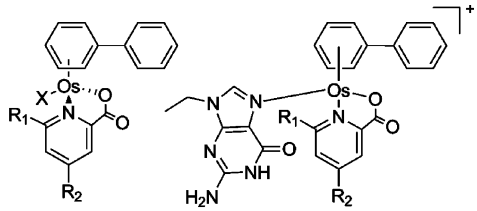

X=Cl	X=D_2O	R_1	R_2		R_1	R_2
1	1A	Br	H	9EtG-3	Me	H
2	2A	OH	H	9EtG-4	H	Cl
3	3A	Me	H	9EtG-5	H	CO_2H
4	4A	H	Cl	9EtG-6	H	Me
5	5A	H	CO_2H			
6	6A	H	Me			
7	7A	H	CO_2Et			

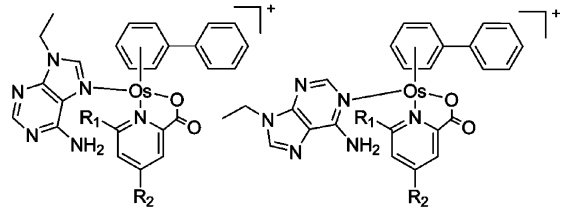

	R_1	R_2		R_1	R_2
9EtA-1a	Br	H	9EtA-1b	Br	H
9EtA-2a	OH	H	9EtA-2b	OH	H
9EtA-3	Me	H			
9EtA-4	H	Cl			
9EtA-5	H	CO_2H			
9EtA-6	H	Me			

of the Ru^{II} analogue. This highlights the lower reactivity of Os^{II}.[2] Interestingly, despite its slow hydrolysis rate, $[(\eta^6$-biphenyl)Os(en)Cl$]^+$ still exhibits promising activity against the human ovarian cancer A2780 cell line ($IC_{50} = 9\ \mu M$).[3b] Changing the ligand from the neutral *N*,*N*-chelator en to the anionic *O*,*O*-chelator acetylacetonate (acac) has a marked effect on the extent and rate of hydrolysis. The hydrolysis rate of $[(\eta^6$-arene)Os(acac)Cl], is too fast to monitor by NMR at 298 K. However, hydrolysis of the acac compounds is complicated by the formation of the hydroxo bridged dimer, $[(\eta^6$-arene)Os$(\mu^2$-OH$)_3$Os$(\eta^6$-arene)$]^+$, with loss of the acac ligand. This hydroxo-bridged dimer is the only observed species at the micromolar concentrations in solutions similar to those used in biological cell culture tests.[2] On account of formation of these hydroxo-bridged adducts, compounds containing *O*,*O*-chelators are generally inactive toward the human ovarian (A2780) and human lung (A549) cancer cell lines.

Intermediate behavior to that of the complexes containing *N*,*N*- and *O*,*O*-chelators is observed in aqueous solution for some complexes containing anionic *N*,*O*-chelators. Complexes containing a pyridine derivative as the N-donor atom hydrolyze at an intermediate rate, are stable in aqueous solution at micromolar concentrations, and are active toward both A549 and A2780 cell lines.[3] Notably, complexes containing picolinate (pico) as the *N*,*O*-chelate, display promising activity toward the human ovarian cancer cell line with $IC_{50} = 4.5\ \mu M$, a value similar to that of carboplatin ($IC_{50} = 6\ \mu M$). These studies demonstrate that the kinetics and thermodynamics of these types of complexes are significant for their biological activity and importantly, that these factors can be controlled by appropriate ligand design. Here we investigate the optimization of the biological activity of osmium(II) arene complexes where YZ is a picolinate derivative (Chart 1). This has been approached by making systematic changes to their design by placing different substituents in the *ortho*- and *para*-positions of the pyridine ring of the picolinate chelating ligand. Solid-state structures, cytotoxicity data, and investigations of their aqueous chemistry using ^{1}H NMR spectroscopy, including their rates of hydrolysis, acidity of the resulting aqua adducts, and nucleobase binding studies, are discussed. This work shows that substituents on the picolinate backbone can have significant effects on the aqueous chemistry in osmium(II) compounds of the type $[(\eta^6$-bip)Os(YZ)(Cl)] providing great scope for design for this class of compounds.

Experimental Section

Materials. 1,4-Dihydrobiphenyl and the dimer, $[(\eta^6$-bip)$OsCl_2]_2$ were prepared by previously reported procedures.[2,4] 9-Ethyl guanine and 9-ethyl adenine were purchased from Sigma-Aldrich. $OsCl_3 \cdot nH_2O$ and 6-hydroxo picolinic acid (>97%) were purchased from Alfa Aesar. 2-Cyano-4-methyl pyridine (98%) and thionyl chloride were obtained from Riedel de Haën and Fluka, respectively. 6-Bromo picolinic acid (98%), 6-methyl picolinic acid (95%), 2,4 pyridinedicarboxylic acid monohydrate (98%), dicyclohexylcarbodiimide, and all deuterated solvents were obtained from Aldrich. Ethanol and methanol were distilled over magnesium/iodine prior to use.

Preparation of Complexes. Complexes **1**−**6** were synthesized from the dimeric precursor, $[(\eta^6$-bip)$OsCl_2]_2$, using procedures similar to those reported previously for other half-sandwich Os^{II} arene complexes.[5,6] Complex **7** was synthesized in EtOH using dicyclohexylcarbodiimide (DCC) as coupling reagent.

4-Chloro Picolinic Acid. A suspension of picolinic acid (0.79 g, 6.35 mmol) and sodium bromide (1.30 g, 12.7 mmol) in 10 mL of thionyl chloride was refluxed mildly for 20 h. The initially dark green mixture changed to a dark red color. Excess $SOCl_2$ was removed by rotary evaporation, and the orange residue was taken up in about 15 mL of CH_2Cl_2 and was filtered through celite to remove any insoluble material. The orange solution was cooled to 271 K, and 20 mL of H_2O (doubly distilled) was added dropwise while stirring vigorously, keeping the temperature between 271 and 275 K. The color of the solution changed to a lighter orange, and a white precipitate formed. The mixture was further stirred at ambient temperature for 20 h. The CH_2Cl_2 and H_2O were removed by rotary evaporation. The solid was recrystallized from a minimum amount of EtOH to give a yield of 0.28 g (28%). ^{1}H NMR (DMSO-d_6): $\delta = 8.72$ (1 H, d, $J = 4.9$ Hz), 8.09 (1 H, d, $J = 1.6$ Hz), 7.84 (1 H, dd, $J = 4.9, 1.6$ Hz).

4-Methyl Picolinic Acid. A solution of 2-cyano-4-methyl pyridine (0.15 g, 1.27 mmol) in about 10 mL of 6 M HCl was refluxed for 24 h. During this time, the initially light yellow solution

(4) Stahl, S.; Werner, H. *Organometallics* **1990**, *9*, 1876.
(5) Morris, R. E.; Aird, R. E.; Murdoch, P. D.; Chen, H. M.; Cummings, J.; Hughes, N. D.; Parsons, S.; Parkin, A.; Boyd, G.; Jodrell, D. I.; Sadler, P. J. *J. Med. Chem.* **2001**, *44*, 3616.
(6) Fernandez, R.; Melchart, M.; Habtemariam, A.; Parsons, S.; Sadler, P. L. *Chem.*−*Eur. J.* **2004**, *10*, 5173.

changed to a clear solution. The solution was taken to dryness, and a white solid remained. The solid was recrystallized from a minimal amount of distilled water to give a yield of 148 mg (85%). ^{1}H NMR (DMSO-d_6): δ = 8.65 (1H, s), 8.06 (1H, s), 7.66 (1H, s), 2.05 (3H, s).

[(η^6-bip)Os(6-Br-pico)Cl] (1). A solution of [(η^6-bip)$OsCl_2$]$_2$ (51.9 mg, 0.06 mmol) in dry and degassed MeOH (10 mL) was refluxed under argon for 1 h before adding a solution of sodium methoxide (2.2 mol equiv, 7.2 mg) and 6-bromo picolinic acid (2.2 mol equiv, 27.2 mg) in 5 mL of dry and degassed MeOH. The resulting mixture was refluxed mildly for 3 h, filtered, and solvent reduced on a rotary evaporator until precipitate began to form and was left standing at 278 K. The yellow powder was recovered by filtration and was air-dried to give a final yield of 45.6 mg (63%). Anal. Calcd for $C_{18}H_{13}BrClNO_2Os$ (580.94): C, 37.22; H, 2.26; N, 2.41%. Found: C, 36.91; H, 2.12; N, 2.25%. ^{1}H NMR ($CDCl_3$): δ = 8.09 (1H, d, J = 7.0 Hz), 7.83 (1H, d, J = 7.0 Hz), 7.70 (1H, t, 8 Hz), 7.52 (2H, d, J = 7.9 Hz), 7.38 (3H, m), 6.71 (1H, d, J = 5 Hz), 6.63 (1H, d, J = 6 Hz), 6.46 (1H, t, J = 5.29 Hz), 6.35 (1H, t, J = 6.0 Hz), 6.32 (1H, t, J = 5.29 Hz). Crystals suitable for X-ray diffraction were obtained by slow evaporation from $CHCl_3$ as **1**·$CHCl_3$ at ambient temperature.

[(η^6-bip)Os(6-OH-pico)Cl] (2). Synthesis as for **1** using [(η^6-bip)$OsCl_2$]$_2$ (51.7 mg, 0.06 mmol), sodium methoxide (2.2 equiv, 6.71 mg), and 6-hydroxo picolinic acid (2.2 equiv, 19 mg). Yield: 37.3 mg (60%). Calcd for $C_{18}H_{14}ClNO_3Os$ (517.99): C, 41.74; H, 2.72; N, 2.70%. Found: C, 41.22; H, 2.62; N, 2.65%. ^{1}H NMR (DMSO-d_6): δ =13.12 (1H, br), 7.86 (1H, t, J = 8 Hz), 7.65 (2H, d, J = 7.2 Hz), 7.44 (3H, m), 7.33 (1H, d, J = 7.0 Hz), 7.11 (1H, d, J = 8.31 Hz), 6.74 (1H, d, J = 5.29 Hz), 6.66 (1H, d, J = 5.28 Hz), 6.42 (2H, m), 6.38 (1H, t, J = 4.53 Hz).

[(η^6-bip)Os(6-Me-pico)Cl] (3). Synthesis as for **1** using [(η^6-bip)$OsCl_2$]$_2$ (52.2 mg, 0.06 mmol), sodium methoxide (2.2 mol equiv, 7.0 mg), and 6-methyl picolinic acid (2.2 mol equiv, 18 mg). Yield: 50 mg (77%) Anal. Calcd for $C_{19}H_{16}ClNO_2Os$ (517.05): C, 44.22; H, 3.13; N, 2.71%. Found: C, 43.89; H, 2.65; N, 2.73%. ^{1}H NMR ($CDCl_3$): δ = 7.95 (1H, d, J = 7.93 Hz), 7.72 (1H, t, J = 7.56), 7.43 (3H, m), 7.36 (3H, m), 6.51 (1H, d, J = 5.29 Hz), 6.47 (1H, d, J = 5.67 Hz), 6.30 (1H, t, J = 5.29 Hz), 6.27 (1H, t, J = 4.91 Hz), 6.22 (1H, t, J = 5.29 Hz).

[(η^6-bip)Os(4-Cl-pico)Cl] (4). Synthesis as for **1** using [(η^6-bip)$OsCl_2$]$_2$ (51.5 mg, 0.06 mmol), sodium methoxide (2.2 mol equiv, 7.4 mg), and 4-chloro picolinic acid (2.2 mol equiv, 21.5 mg). Yield: 37.1 mg (54%) Anal. Calcd for $C_{18}H_{13}Cl_2NO_2Os$·H_2O (554.45): C, 38.99; H, 2.73; N, 2.53%. Found: C, 38.66; H, 1.95; N, 2.60%. ^{1}H NMR (DMSO-d_6): δ = 9.11 (1H, d, J = 5.67 Hz), 7.93 (1H, d, J = 1.89 Hz), 7.92 (1H, dd, J = 6.04, 2.26 Hz), 7.65 (2H, m), 7.47 (3H, m), 6.76 (1H, d, J = 5.29 Hz), 6.72 (1H, d, J = 5.66), 6.46 (1H, t, J = 5.29 Hz), 6.43 (1H, t, J = 5.29 Hz), 6.40 (1H, t, J = 4.91 Hz).

[(η^6-bip)Os(4-CO_2H-pico)Cl] (5). Synthesis as for **1** using [(η^6-bip)$OsCl_2$]$_2$ (53.6 mg, 0.06 mmol), sodium methoxide (2.2 mol equiv, 7.3 mg), and 2,4 pyridinedicarboxylic acid (2.2 mol equiv, 23.3 mg). Yield: 29.7 mg (41%). Anal. Calcd for $C_{19}H_{14}ClNO_4Os$ (546.00): C, 41.80; H, 2.58; N, 2.57%. Found: C, 41.19; H, 2.12; N, 2.55%. ^{1}H NMR (DMSO-d_6): δ = 9.31 (1H, m), 8.14 (1H, m), 8.01 (1H, m), 7.65 (2H, m), 7.47 (3H, m), 6.76 (1H, d, J = 5.67 Hz), 6.72 (1H, d, J = 6.04 Hz), 6.46 (1H, t, J = 5.29 Hz), 6.44 (1H, t, J = 5.29 Hz), 6.41 (1H, t, J = 4.91 Hz).

[(η^6-bip)Os(4-Me-pico)Cl] (6). Synthesis as for **1** using [(η^6-bip)$OsCl_2$]$_2$ (53.1 mg, 0.06 mmol), sodium methoxide (2.2 mol equiv, 7.4 mg), and 4-methyl picolinic acid (2.2 mol equiv, 19.2 mg). Yield: 35.6 mg (57%) Anal. Calcd for $C_{19}H_{16}ClNO_2Os$·H_2O (534.03): C, 42.73; H, 3.40; N, 2.62%. Found: C, 42.57; H, 2.99; N, 2.58%. ^{1}H NMR (DMSO-d_6): δ = 8.94 (1H, d, J = 5.66 Hz), 7.74 (1H, br), 7.63 (2H, m), 7.52 (1H, d, J = 4.53 Hz), 7.45 (3H, m), 6.73 (1H, d, J = 5.29 Hz), 6.69 (1H, d, J = 4.91 Hz), 6.40 (1H, m), 6.37 (2H, m). Crystals suitable for X-ray diffraction were obtained by slow evaporation from CH_2Cl_2 as **6**·CH_2Cl_2 at ambient temperature.

[(η^6-bip)Os(4-CO_2Et-pico)Cl] (7). A solution of [(η^6-bip)$OsCl_2$]$_2$ (47.1 mg, 0.056 mmol) and dimethylaminopyridine (3 mg) in dry and degassed EtOH was placed under nitrogen and was stirred for 10 min after which it was cooled down to 273 K before adding dicyclohexylcarbodiimide (1 mol equiv, 19 mg). The reaction mixture was stirred at 273 K for a further 15 min, after which it was left to stir at ambient temperature for another 2.5 h. This was then filtered, and the solvent was removed on the rotary evaporator. About 3 mL of dry DCM was added to the brown solid, and this was filtered to remove the white precipitated urea side product. The DCM filtrate was dried on a rotary evaporator, and the brown solid was washed with ether to remove the remaining dimethylaminopyridine which resulted in a brown crystalline solid. Yield 2.2 mg (3.4%). ^{1}H NMR (MeOD-d_4): δ = 9.10 (1H, d, J = 5.52 Hz), 8.40 (1H, d, J = 1.76 Hz), 8.05 (1H, dd, J = 3.76, 2.01 Hz), 7.64 (2H, m), 7.44 (3H, m), 6.70 (1H, d, J = 5.02 Hz), 6.66 (1H, d, J = 5.77 Hz), 6.39 (2H, q, J = 4.76 Hz), 6.34 (1H, m), 4.48 (2H, q, J = 7.03 Hz), 1.2 (3H, t, J = 7.03 Hz).

Instrumentation. X-ray Crystallography. Diffraction data for compound **1** were collected at 150 K using a Bruker Smart Apex CCD diffractometer. Diffraction data for **6** was collected at 120 K by the EPSRC National Crystallography Service (Southampton) using a Bruker-Nonius APEX II CCD camera on kappa-goniostat. Absorption corrections for all data sets were performed with the multiscan procedure SADABS.[7] The structure of **1** was solved by direct methods (SIR92),[8] and that of **6** by Patterson methods (DIRDIF).[9] Refinement was against F^2 using all data (SHELX-TL).[10] H-atoms were placed in geometrically calculated positions. In **6** a molecule of dichloromethane is disordered about a crystallographic inversion center. The C−Cl bond distances were restrained to 1.73(1) Å during refinement. The programs Diamond 3.020,[11] Mercury 1.4.1,[12] and ORTEP 32[13] were used for analysis of data and production of graphics. X-ray crystallographic data for compounds **1** and **6** have been deposited in the Cambridge Crystallographic Data Centre under the accession numbers CCDC 706164 and 706165, respectively.

NMR Spectroscopy. ^{1}H NMR spectra were acquired in 5 mm NMR tubes at 298 K (unless stated otherwise) on either a Bruker DMX 500 (^{1}H = 500.13 MHz) or an AVA 600 (^{1}H = 599.81 MHz) spectrometer. ^{1}H NMR chemical shifts were internally referenced to (C*H*D$_2$)(CD$_3$)SO (2.50 ppm) for DMSO-d_6, C*H*Cl$_3$ (7.26 ppm) for chloroform-d_1, and to 1,4-dioxane (3.75 ppm) for aqueous solutions. For NMR spectra of aqueous solutions, water suppression

(7) Sheldrick, G. M. *SADABS*, Version 2006−1; University of Göttingen: Göttingen, Germany, 2006.
(8) Altomare, A.; Cascarano, G.; Giacovazzo, C.; Guagliardi, A. *J. Appl. Crystallogr.* **1994**, *27*, 1045.
(9) Beurskens, P. T., Beurskens, G.; Bosman, W. P.; de Gelder, R.; Garcia-Granda; S.; Gould, R. O.; Israel, R.; Smits, J. M. M. *Crystallography Laboratory*; University of Nijmegen: The Netherlands, 1996.
(10) Sheldrick, G. M. *SHELXL-97. Program for the refinement of crystal structures*; University of Göttingen: Germany, 1997.
(11) *CrystalImpact DIAMOND, version 3.0, Visual crystal structure information system.*; Crystal Impact GbR: Bonn, Germany, 2004.
(12) Macrae, C. F.; Edgington, P. R.; McCabe, P.; Pidcock, E.; Shields, G. P.; Taylor, R.; Towler, M.; van de Streek, J. *J. Appl. Crystallogr.* **2006**, *39*, 453.
(13) Farrugia, L. J. *J. Appl. Crystallogr.* **1997**, *30*, 565.

was carried out using Shaka or presaturation methods. [14] All data processing was carried out using XWIN-NMR version 3.6 (Bruker U.K. Ltd.).

pH* Measurements. pH* values (pH meter reading without correction for effects of D on glass electrode) of NMR samples in D_2O were measured at about 298 K directly in the NMR tube, before and after recording NMR spectra, using a Corning 240 pH meter equipped with a micro combination electrode calibrated with Aldrich buffer solutions of pH 4, 7, and 10.

Elemental Analysis. Carbon, hydrogen, and nitrogen (CHN) elemental analysis were carried out at The University of St. Andrews in the School of Chemistry on a Carlo Erba CHNS analyzer.

Methods. Kinetics of Hydrolysis. The kinetics of hydrolysis for complexes **1**−**6** were followed by ^{1}H NMR at different temperatures. For this, solutions of the complexes with a final concentration of 0.8 mM in 5% MeOD-d_4/95% D_2O (v/v) were prepared by dissolution of the complexes in MeOD-d_4 followed by rapid dilution using D_2O with a pH* of about 2 (acidified with HNO_3), so that the aqua ligand was not deprotonated. ^{1}H NMR spectra were taken after various intervals using the presaturation method for water surpression. The rate of hydrolysis was determined by fitting plots of concentrations (determined from ^{1}H NMR peak integrals) versus time to a pseudo first-order equation using ORIGIN version 5.0 (Microcal Software Ltd.). The Arrhenius activation energy (E_a), activation enthalpies ($\Delta H^{\ddagger}$), and activation entropy ($\Delta S^{\ddagger}$) for compound **6** were determined from the slopes of the Arrhenius and intercepts of Eyring plots.

pK_a* Calculations. For determinations of pK_a* values (pK_a values determined from solutions in D_2O), the pH* values of the aqua complexes of **3**−**6** in D_2O (formed in situ by dissolution of the parent chloro complexes) were varied from about pH* 2 to 10 by the addition of dilute NaOD and HNO_3, and ^{1}H NMR spectra were recorded. The chemical shifts of the arene ring protons were plotted against pH*. The pH* titration curves were fitted to the Henderson−Hasselbalch equation, with the assumption that the observed chemical shifts are weighted averages according to the populations of the protonated and deprotonated species. These pK_a* values can be converted to pK_a values by use of the equation pK_a = 0.929pK_a* + 0.42 as suggested by Krezel and Bal[15] for comparison with related values in the literature.

Interactions with Nucleobases. The reaction of **1**−**6** with nucleobases typically involved addition of a solution containing 1 mol equiv of nucleobase in D_2O, to an equilibrium solution of **1**−**6** in D_2O (>90% aqua complex). The pH* value of the sample was adjusted if necessary so as to remain close to 7.4 (physiological). ^{1}H NMR spectra of these solutions were recorded at 298 K after various time intervals.

Cancer Cell Cytotoxicity. After plating, human ovarian A2780 and cisplatin resistant A2780cis cancer cells were treated with Os^{II} complexes on day 3, and human lung A549 and human colon HCT116 cancer cells on day 2, at concentrations ranging from 0.5 μM to 100 μM. Solutions of the Os^{II} complexes were made up in 0.125% (v/v) dimethylsulfoxide (DMSO) to assist dissolution (0.03% final concentration of DMSO per well in the 96-well plate). Cells were exposed to the complexes for 24 h, washed, supplied with fresh medium, allowed to grow for three doubling times (72 h), and then the protein content measured (proportional to cell survival) using the sulforhodamine B (SRB) assay.[16]

Computation. Density-functional theory (DFT) calculations were carried out by using the Amsterdam density functional (ADF)[17] program (version 2007.01). The coordinates of complexes used for the calculations were obtained directly from the X-ray crystal structures. Modifications to the structures were performed in Chemcraft (version 1.5). Geometries and energies were obtained by using the Perdew−Wang gradient-corrected functional (GGA) with scalar ZORA relativistic correction.[18−22] The general numerical intergration was 4.0. The frozen core approximation[23] was applied using triple-ζ polarization (TZP). Default convergence criteria were applied for self-consistent fields (SCF) and geometry optimization. The COSMO, as implemented in ADF program, was used to simulate the aqueous environment with ε = 78.4 and a probe radius = 1.9 Å. The atomic radii used were Os = 1.958, F = 1.425, Cl = 1.725, Br = 1.850, O = 1.517, N = 1.608, C = 1.700, and H = 1.350 Å.

Results

Synthesis and Characterization. The osmium compounds were synthesized via the Cl-bridged dimer, $[(\eta^6\text{-bip})OsCl_2]_2$, where bip = biphenyl. Compound **7,** however, was obtained in low yield from compound **5** as starting material in dry ethanol with DCC as coupling reagent. The X-ray crystal structures of compounds $[(\eta^6\text{-bip})Os(6\text{-Br-pico})Cl]\cdot CHCl_3$ (**1**·$CHCl_3$) and $[(\eta^6\text{-bip})Os(4\text{-Me-pico})Cl]\cdot CH_2Cl_2$ (**6**·CH_2Cl_2) were determined. Both structures adopt the familiar pseudo-octahedral "three-leg piano stool" geometry (Figure 1A,B). The osmium is π-bonded to the arene ligand ("the seat") with a centroid Os-ring distance of 1.654 Å for **1** and 1.660 Å for **6**, σ-bonded to the chloride (2.4065(15) Å (**1**), 2.4095(19) Å (**6**)) and σ-bonded to the chelating picolinate ligand (pyridine nitrogen-Os; 2.154(5) Å (**1**), 2.088(5) Å (**6**), oxygen-Os 2.077(4) Å (1), 2.082(4) Å (**6**)), which constitute the three legs of the piano stool. Crystallographic data, selected bond lengths, and angles are given in Tables 1 and 2. Complex **1** has a propeller twist of the biphenyl ligand of about 38°, while for complex **6** a propeller twist of 42° is observed. There is an intermolecular interaction between the outer rings of the biphenyl arene of adjacent molecules in compound **6**, with a centroid−centroid distance of 3.7 Å (Figure 2). This value indicates intermolecular ring stacking.[24]

Kinetics of Hydrolysis. The rates of hydrolysis of compounds **1**−**6** in a 5% MeOD-d_4/95% D_2O were monitored by ^{1}H NMR at 288 and 298 K by the observation of new peaks over time due to aqua adduct formation. Five percent MeOD was used to improve solubility, and acidic

(14) Hwang, T. L.; Shaka, A. J. *J. Magn. Reson. Ser. A* **1995**, *112*, 275.
(15) Krezel, A.; Bal, W. *J. Inorg. Biochem.* **2004**, *98*, 161.
(16) Skehan, P.; Storeng, R.; Scudiero, D.; Monks, A.; McMahon, J.; Vistica, D.; Warren, J. T.; Bokesch, H.; Kenney, S.; Boyd, M. R. *J. Natl. Cancer Inst.* **1990**, *82*, 1107.
(17) Te Velde, G.; Bickelhaupt, F. M.; Baerends, E. J.; Fonseca Guerra, C.; Van Gisbergen, S. J. A.; Snijders, J. G.; Ziegler, T. *J. Comput. Chem.* **2001**, *22*, 931.
(18) van Lenthe, E.; Baerends, E. J.; Snijders, J. G. *J. Chem. Phys.* **1993**, *99*, 4597.
(19) van Lenthe, E.; Baerends, E. J.; Snijders, J. G. *J. Chem. Phys.* **1994**, *101*, 9783.
(20) van Lenthe, E.; Baerends, E. J.; Snijders, J. G. *J. Chem. Phys.* **1996**, *105*, 2373.
(21) van Lenthe, E.; Ehlers, A.; Baerends, E.-J. *J. Chem. Phys.* **1999**, *110*, 8943.
(22) van Lenthe, E.; van Leeuwen, R.; Baerends, E. J.; Snijders, J. G. *Int. J. Quantum Chem.* **1996**, *57*, 281.
(23) Baerends, E. J.; Ellis, D. E.; Ros, P. *Theor. Chim. Acta* **1972**, *27*, 339.
(24) Janiak, C. *J. Chem. Soc., Dalton Trans.* **2000**, 3885.

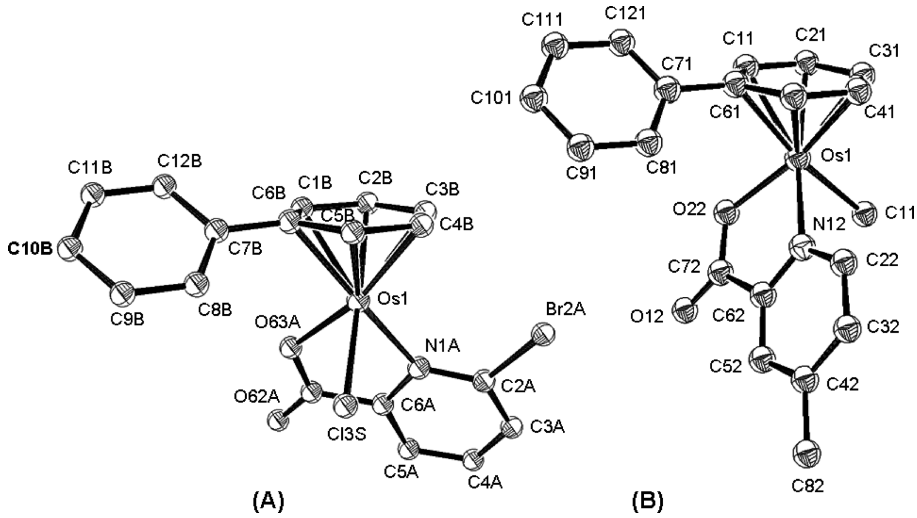

Figure 1. X-ray crystal structure and atom numbering scheme for (A) [(η^6-bip)Os(6-Br-pico)Cl]·$CHCl_3$ (**1**·$CHCl_3$), and (B) [(η^6-bip)Os(4-Me-pico)Cl]·CH_2Cl_2 (**6**·CH_2Cl_2). H atoms and solvent molecules have been omitted for clarity.

Table 1. Crystallographic Data for [(η^6-bip)Os(2-Br-pico)Cl]·$CHCl_3$ (**1**·$CHCl_3$) and [(η^6-bip)Os(4-Me-pico)Cl]·CH_2Cl_2 (**6**·CH_2Cl_2)

	1·$CHCl_3$	**6**·CH_2Cl_2
formula	C_{19} H_{14} Br Cl_4 N O_2 Os	C_{19} H_{16} Cl N O_2 Os
molecular weight	700.22	558.44
crystal description	colorless block	colorless lath
size	0.34 × 0.17 × 0.14 mm	0.16 × 0.06 × 0.02 mm
λ (Å)	0.71073	0.71073
T/K	150(2)	120(2)
crystal system	triclinic	triclinic
space group	$P\bar{1}$	$P\bar{1}$
a (Å)	6.8555(8)	8.065(5)
b (Å)	11.0638(11)	10.495(5)
c (Å)	13.9209(19) A	11.672(5)
α (deg)	99.783(7)	81.806(5)
β (deg)	98.387(8)	78.860(5)
γ (deg)	91.757(7)	77.776(5)
volume ($Å^3$)	1027.7(2)	942.0(8)
Z	2	2
R	0.0376	0.0399
R_w	0.0868	0.0837
GOF	0.997	1.120

Table 2. Selected Bond Lengths (Å) and Angles (deg) for [(η^6-bip)Os(2-Br-pico)Cl]·$CHCl_3$ (**1**·$CHCl_3$) and [(η^6-bip)Os(4-Me-pico)Cl]·CH_2Cl_2 (**6**·CH_2Cl_2)

bond length/ angle	compound **1**·$CHCl_3$	compound **6**·CH_2Cl_2
Os−C(arene)	2.178(7)	2.164(6)
	2.207(7)	2.208(7)
	2.175(6)	2.193(6)
	2.177(6)	2.199(6)
	2.159(6)	2.173(6)
	2.208(6)	2.176(6)
Os−O	2.077(4)	2.082(4)
Os−N	2.154(5)	2.088(5)
Os−Cl	2.4065(15)	2.4095(19)
O−Os−N	77.35(18)	77.10(18)
O−Os−Cl	84.82(12)	84.50(14)
N−Os−Cl	81.74(13)	83.30(15)

conditions (D_2O, pH* 2) were used to prevent the deprotonation of the aqua complex as a secondary reaction. The hydrolysis of compound **2** containing 6-hydroxy picolinate was too rapid to be observed by ^{1}H NMR at 288 K. The percentage of aqua peak formation for **1**, **3**−**6** was plotted against time and was fitted to pseudofirst order kinetics (Figure 3, Supporting Information, Figure S1), and their half-life times were calculated (Table 3). The Arrhenius activation

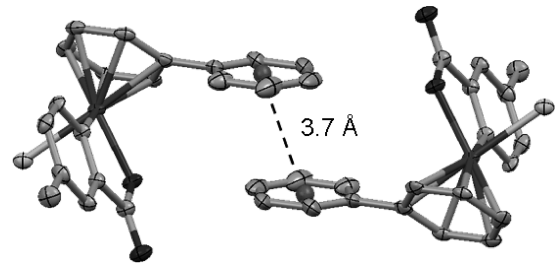

Figure 2. X-ray structure of [(η^6-bip)Os(4-Me-pico)Cl]·CH_2Cl_2 (**6**·CH_2Cl_2) showing intermolecular ring stacking of the extended biphenyl ring.

energy (E_a), activation enthalpy ($\Delta H^{\ddagger}$), and activation entropy ($\Delta S^{\ddagger}$) of compound **6** (Figure 3B) are listed in Table 4. The large negative $\Delta S^{\ddagger}$ value for compound **6** is notable. The extent of hydrolysis at equilibrium is high for all compounds, with even 100% hydrolysis observed for compounds **4** and **5** and between 88% and 96% for **1**, **3**, and **6** (Figure 3A,B). The hydrolysis rate of compound **1** (6-Br pico) was too slow to monitor at 288 K, but its half-life was successfully determined by increasing the temperature to 298 K (Table 3, Figure 3A). Compound **6** hydrolyzes the fastest with a half-life of just under 1 h (288 K). Complexes **1**, **3**−**5** hydrolyzed with half-lives ranging from 2.4 to 4.4 h at 288 K (Table 3).

The effects of chloride concentrations typical of blood plasma (100 mM), cell cytoplasm (22.7 mM), and cell nucleus (4 mM) on the aqueous chemistry of **3** and **6** were investigated. ^{1}H NMR spectra of **3** or **6** (1 mM) were recorded within 10 min of sample preparation and after incubation at 310 K for 24 h (Supporting Information, Figure S2). On the basis of ^{1}H NMR peak integrals, 35% of hydrolyzed complex **3** (**3A**) and 10% of hydrolyzed complex **6** (**6A**) were found to be present in 100 mM [Cl] (pH* 6.22), 60% of **3A**, and 53% of **6A** at 22.7 mM [Cl] (pH* 6.50) and 60% of **3A** and 82% of **6A** at 4 mM [Cl] (pH* 6.75) after 10 min. For complex **6**, no significant change was observed after 24 h, while compound **3** had not reached equilibrium after 24 h, see Table 5 and Supporting Information, Figure S2.

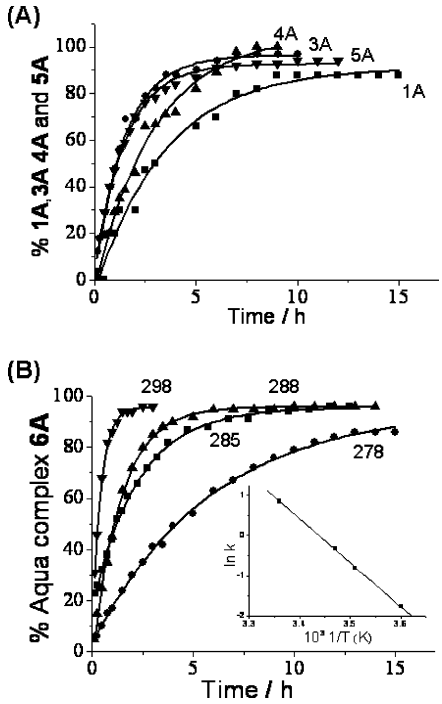

Figure 3. Time dependence for formation of the aqua complexes **1A**, **3A**, **4A**, **5A**, and **6A** (based on ^{1}H NMR peak integrals) during hydrolysis of **1**, **3**, **4**, and **5** in acidic D_2O (pH* 2) at (A) 298 K for **1A** (■), **3A** (●), **4A** (▲), and **5A** (▼) and (B) at 298 K (▼), 288 K (▲), 285 K (■), and 278 K (●) for **6A**. The inset shows the Arrhenius plot, the slope of which gives the Arrhenius activation energy E_a of 90.6 kJ mol^{-1}.

Table 3. Hydrolysis Data for Compounds **1**−**6** at 288 K/ 298 K, Determined by ^{1}H NMR

compound	*T*/ K	*k*/ h^{-1}	$t_{1/2}$/ h
1	298	0.345 ± 0.0002	2.01 ± 0.001
2	288	≥5.9	≤0.12
3	288	0.219 ± 0.005	3.17 ± 0.07
	298	0.676 ± 0.039	1.03 ± 0.04
4	288	0.288 ± 0.001	2.40 ± 0.08
	298	0.656 ± 0.032	1.06 ± 0.05
5	288	0.158 ± 0.011	4.42 ± 0.32
	298	0.384 ± 0.004	1.81 ± 0.02
6	288	0.710 ± 0.012	0.98 ± 0.02
	298	2.32 ± 0.08	0.30 ± 0.01

pK_a* Determination. The changes in the ^{1}H NMR chemical shifts for the protons of the coordinated phenyl ring in compounds **3**−**6**, present in equilibrium solutions of **3**−**6** with their aqua adducts as the major species (**3A**−**6A**), were followed with change in pH* over a range of 2−10 (Supporting Information, Figure S3A). When the pH* values of the solutions were increased from about 2 to 10, the major set of NMR peaks assigned to **3A**, **4A**, and **6A** gradually shifted to high field in the spectrum. In contrast, the signals assignable to parent chloro species **3**, **4**, and **6** remained unchanged with changing pH*, but their intensities increased at lower pH*. The protonation of the *para*-carboxylate on the picolinate ring of complex **5** caused the NMR peaks assigned to both species (**5** and **5A**) to shift to high field at low pH* (Supporting Information, Figure S3B), while at higher pH* only the peaks assignable to **5A** shifted to higher field.

Because of the chirality at the osmium metal center, none of the protons of the coordinated arene are equivalent, and each gave rise to separate ^{1}H NMR peaks at high and low pH. The chemical shifts were plotted against pH*, Supporting Information, Figure S4, and the resulting pH titration curves were fitted to the modified Henderson−Hasselbalch equation.[25,26] This gave rise to pK_a* values between 6.30 and 6.60 (Table 6). For compound **5**, the pK_a* value of the *para*-substituent carboxylic acid proton was determined to be 2.50.

Reactions with Nucleobase Models, 9-Ethyl Guanine (9EtG) and 9-Ethyl Adenine (9EtA). Since DNA is often believed to be the main target for transition metal anticancer drugs,[27] nucleobase binding reactions of compounds **1**, [(η^6-bip)Os(6-Br-pico)Cl], **2**, [(η^6-bip)Os(6-OH-pico)Cl], **3**, [(η^6-bip)Os(6-Me-pico)Cl], **4**, [(η^6-bip)Os(4-Cl-pico)Cl], **5**, [(η^6-bip)Os(4-CO_2^--pico)Cl], and **6**, [(η^6-bip)Os(4-Me-pico)Cl], with nucleobase models 9-ethyl guanine (9EtG) and 9-ethyl adenine (9EtA), were investigated. Solutions of **1**−**6** (1 mM) (containing an equilibrium mixture of **1**−**6** and their respective aqua adducts **1A**−**6A** as the major species) with 1 mol equivalent of 9EtG or 9EtA in D_2O were prepared, and ^{1}H NMR spectra were recorded at different time intervals. The percentages of nucleobase adducts formed by all compounds based on ^{1}H NMR peak integrals are displayed in Table 7A,B and Figure 4. The addition of 1 mol equiv 9EtG or 1 mol equiv 9EtA to aqueous solutions of all compounds resulted in no new peaks after about 5 min. However, after incubation at 310 K for 24 h, new peaks for all compounds were observed.

Compounds **4**-**6** formed 9EtG and 9EtA adducts to the extent of 60%−100% completion after 24 h. Only compound **6** showed increased binding to 9EtG, with 20% more binding compared to 9EtA. Compound **5** showed an exceptionally high nucleobase affinity with 100% nucleobase adduct formation with both 9EtG and 9EtA after 24 h. The *ortho*-substituted pico compounds **1**−**3** were less reactive toward the nucleobases compared to the *para*-substituted compounds **4**−**6** (Table 7, Figure 4). Compound **3** (*o*-Me) showed a preference for 9EtG, while compounds **1** (*o*-Br) and **2** (*o*-OH) formed no adducts with 9EtG, but did form 9EtA adducts. In contrast to compounds **3**−**6**, compounds **1** and **2** formed two adenine nucleobase adducts, most likely through osmium binding to the N1 or N7 of adenine forming **9EtA-1/2a** and **b**, Chart 1. It was not possible to determine the precise adduct ratio for **9EtA-1** adducts because of peak overlap. Compound **2** formed 9EtA adducts in a 14% and 22% ratio.

Cytotoxicity Data. The cytotoxicity of complexes **1**−**7** toward colon HCT116, human lung A549, ovarian A2780, and ovarian cisplatin-resistant A2780cis cancer cell lines was investigated (Table 8). Complexes **1**, **2**, **3**, and **5** were nontoxic up to the highest test concentration of 50 μM in all four cell lines. The IC_{50} values (concentration at which 50% of the cell growth is inhibited) of these complexes are

(25) Lee, S. A.; Eyeson, R.; Cheever, M. L.; Geng, J. M.; Verkhusha, V. V.; Burd, C.; Overduin, M.; Kutateladze, T. G. *Proc. Natl. Acad. Sci. U.S.A.* **2005**, *102*, 13052.
(26) Sigel, R. K. O.; Sabat, M.; Freisinger, E.; Mower, A.; Lippert, B. *Inorg. Chem.* **1999**, *38*, 1481.
(27) Zhang, C. X.; Lippard, S. J. *Curr. Opin. Chem. Biol.* **2003**, *7*, 481.
(28) Peacock, A. F. A.; Habtemariam, A.; Moggach, S. A.; Prescimone, A.; Parsons, S.; Sadler, P. *J. Inorg. Chem.* **2007**, *46*, 4049.

Table 4. Rate Data and Activation Parameters for the Aquation of Active Complex **6** at Various Temperatures

compound	T/ K	k/ h^{-1}	$t_{1/2}$/ h	E_a /kJ mol^{-1}	$\Delta H^{\ddagger}$ /kJ mol^{-1}	$\Delta S^{\ddagger}$/J K^{-1} mol^{-1}
6	278	0.17	4.06			
	285	0.44	1.57	90.6±1.0	87.7±2.1	−55.6±1.6
	288	0.71	0.98			
	298	2.32	0.30			

Table 5. Percentage of Aqua Adduct Formation in a Solution of 1 mM **3** or **6** in D_2O at Chloride Levels Typical of Blood Plasma (100 mM), Cell Cytoplasm (22.7 mM), and Cell Nucleus (4 mM)

	% aqua adduct			
	t = 10 min		t = 24 h	
[NaCl]	**3A**	**6A**	**3A**	**6A**
100 mM	35	10	27	20
22.7 mM	60	53	49	53
4 mM	60	82	70	81

Table 6. pK_a* and pK_a Values[a] for the Deprotonation of the Coordinated H_2O in Complexes **3A**−**6A**

complex		pK_a*	pK_a
$[(\eta^6\text{-bip})Os(6\text{-Me-pico})OD_2]^+$	**3A**	6.34	6.31
$[(\eta^6\text{-bip})Os(4\text{-Cl-pico})OD_2]^+$	**4A**	6.30	6.27
$[(\eta^6\text{-bip})Os(4\text{-}CO_2H\text{-pico})OD_2]^+$	**5A**	6.61	6.56
$[(\eta^6\text{-bip})Os(4\text{-Me-pico})OD_2]^+$	**6A**	6.42	6.38

[a] pK_a values calculated from pK_a* according to Krezel and Bal.[15]

Table 7. Extent of 9EtG and 9EtA Adduct Formation for Compounds **1**−**6** at Different Time Intervals

compound	t = 10 min	t = 24 h	t = 72 h
	(A) % 9EtG Nucleobase Adduct		
1	0	0	0
2	0	0	0
3	0	30	30
4	0	59	76
5	0	100	100
6	0	80	85
	(B) % 9EtA Nucleobase Adduct		
1	0	∼30[a]	∼35[a]
2	0	14:20[b]	14:20[b]
3	0	9	9
4	0	62	71
5	0	100	100
6	0	60	60

[a] Approximate value due to peak overlap. [b] Formation of two nucleobase adducts (**9EtA-2a** and **b**, Chart 1).

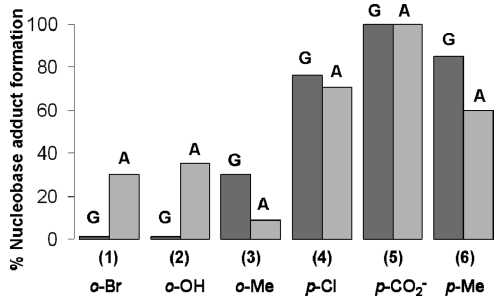

Figure 4. Bar chart showing the extent of binding of compounds **1**−**6** to the nucleobases 9EtG (dark gray) and 9EtA (light gray) after 48 h.

therefore likely to be >100 μM and then can be described as inactive compounds. Compounds **4** (*p*-Cl) and **6** (*p*-Me), however, exhibited promising toxicity with IC_{50} values similar to those found for cisplatin in the human ovarian A2780 and colon HCT116 cancer cell lines and moderate cytotoxicity in the A549 cancer cell line (ca. 3 times less active than cisplatin). Interestingly, both compounds **4** and **6** overcome cisplatin resistance in the A2780cis cell line. Compound **7**, the ethyl ester of compound **5**, shows moderate activity in the human ovarian A2780 and A2780cis cell lines (Table 8).

Table 8. In Vitro Growth Inhibition of A2780, A2780cis, A549, and HCT116 Cell Lines for Compounds **1**−**7** and Cisplatin (CDDP) as Control

compound	A2780 IC_{50} (μM)	A2780cis IC_{50} (μM)	A549 IC_{50} (μM)	HCT116 IC_{50} (μM)
1	>50	>50	>50	>50
2	>50	>50	>50	>50
3	>50	>50	>50	>50
4	4.8	5.45	24	2.8
5	>50	>50	>50	>50
6	4.4	7.61	25.1	2.5
7	44.4	61	ND[a]	ND[a]
CDDP	3	16.9	7.7	2.7

[a] ND = not determined.

Computation. Using computational methods we attempted to gain insight into the steric effects caused by the *ortho* substituents upon nucleobase binding and their effect on the rate of hydrolysis. The minimum energy structures of nucleobase adducts of compounds **1** $[(\eta^6\text{-bip})Os(6\text{-Br-pico})(9EtG/9EtA)]^+$, **3** $[(\eta^6\text{-bip})Os(6\text{-Me-pico})(9EtG/9EtA)]^+$, and **6** $[(\eta^6\text{-bip})Os(4\text{-Me-pico})(9EtG/9EtA)]^+$ obtained from DFT calculations are shown in Supporting Information, Figure S5. The 9EtG adduct of *p*-Me complex **6** is 6.6 kcal/mol lower in energy, and the 9EtA adduct is 5.8 kcal/mol lower in energy compared to similar adducts of its isomer the *o*-Me complex **3**.

Geometry optimizations for the nucleobase adducts of complex **1** revealed H-bonding between the NH_2 of adenine and the caboxylate oxygen of the picolinate ligand (NH···OC, 1.833 Å). In contrast, a close contact between guanine C6O and the ortho-bromide substituent (3.260 Å) was observed in the guanine adduct (Supporting Information, Figure S5).

Discussion

Mixed *N*,*O*-chelating ligands can be used to "fine-tune" the aqueous reactivity of Os^{II} arene compounds by the choice of the types of *N*- and *O*-donor groups. The aim of this study was to optimize the biological activity of osmium(II) arene complexes by making systematic changes to their design using different substituents in the *ortho*- and *para*-positions of the pyridine ring of the picolinate chelating ligand.

Complexes **1**−**7** were synthesized and X-ray structures of compound **1** $[(\eta^6\text{-bip})Os(6\text{-Br-pico})Cl]$, as a $CHCl_3$ solvate, and **6** $[(\eta^6\text{-bip})Os(4\text{-Me-pico})Cl]$, as a CH_2Cl_2 solvate, were determined. Both compounds adopt the familiar pseudo-octahedral "three-leg piano stool" geometry as found previously for other osmium(II) biphenyl compounds (i.e., $[(\eta^6\text{-bip})Os(YZ)(Cl)]$), for which a propeller twist of the biphenyl ligand of about 40° and Os−Cl bond lengths of 2.40 Å are observed.[2]

The π-π stacking by the flexible extended biphenyl arene ring system observed in the X-ray structure of compound **6** (Figure 2) could allow intercalation into DNA to contribute to the cytotoxicity of this class of compounds.

Aqueous Solution Chemistry. Previous studies on the hydrolysis rates of Os^{II} arene compounds of the type $[(\eta^6\text{-arene})Os(YZ)Cl]^{n+}$ have shown that the aqueous reactivity of these complexes is highly dependent on the nature of the chelating ligand YZ.[2,3,28] Compounds **1**−**6** (Chart 1) hydrolyze relatively fast with half-lives ranging from 0.98 to 4.4 h at 288 K, apart from the *o*-OH compound **2**, [(η^6-bip)Os(6-OH-pico)Cl], which hydrolyzes too fast to be monitored by ^{1}H NMR at 288 K (Table 3). In addition, the equilibrium for hydrolysis lies to a great extent toward the aqua adducts for all compounds with even 100% hydrolysis observed for compounds **2**, **4**, and **5**, and between 88% and 96% for **1**, **3**, and **6**. The rapid hydrolysis of compound **2** might be aided by the hydrogen bonding ability of the *ortho*-hydroxo substituent which can stabilize the incoming water molecule in the transition state, and in addition, the electron-donating properties of the *ortho*-hydroxo substituent can contribute to the weakening of the Os−Cl bond.

Compound **6** also hydrolyzes rapidly with a half-life of just under 1 h (288 K), indicating an electronic substituent effect of the *para*-methyl group. The electron-donating properties of the methyl group give rise to increased electron density around osmium which may facilitate chloride loss and therefore result in a faster hydrolysis rate. This substituent effect is also observed for compound **4** which contains the electron-withdrawing (through the inductive effect) *para*-chloride group and for compound **5** with the electron-withdrawing (through the resonance effect) carboxyl group also in the *para*-position on the pyridine ring, with hydrolysis half-lives of 2.4 and 4.4 h (288 K) for **4** and **5**, respectively. A similar trend is observed for compounds **1** and **3** which contain bromide (**1**) and methyl (**3**) substituents in the *ortho*-position of the pyridine ring. Compound **3**, with an electron-donating methyl group, hydrolyzes twice as fast as compound **1**, which contains an electron-withdrawing bromide group. However, important to note is the slower hydrolysis for compound **3** compared to compound **6** (Table 3), both of which contain a methyl substituent but in different positions on the ring (i.e., *ortho* for **3** and *para* for **6**). This can be explained by the steric bulk of the *ortho*-methyl group around the metal center, which may force a less favorable dissociative pathway. A more favorable associative pathway is allowed in the transition state of compound **6** since here the methyl group does not interfere with the reactive site. The large negative activation entropy of hydrolysis (-55.6 J K^{-1} mol^{-1}, Table 4, Figure 3B) for compound **6**, suggests that the mechanism of hydrolysis for this compound does indeed involve an associative pathway.

At high chloride concentrations typical of blood plasma (100 mM), complex **6** is 80% present as the intact chloro species, also referred to as the "prodrug" form since in this form it is relatively unreactive. At a lower chloride concentration resembling that in the cell cytoplasm (22.7 mM), 53% of complex **6** is present in its active hydrolyzed form (**6A**) and at the lowest chloride concentration of 4 mM close to that of the cell nucleus, complex **6** is 81% present as the reactive aqua species. These data indicate that in the cell nucleus, complex **6** might be selectively activated through hydrolysis as a mode of activation toward DNA binding, while outside the cell and in particular in blood plasma complex **6** is predominately present as its less reactive intact chloro species.

For compound **3**, the different chloride concentrations had little effect on the concentration of hydrolyzed complex **3** (**3A**) after 10 min, although after equilibration for 24 h the extent of hydrolysis was similar to that of compound **6**. This can be explained by the steric bulk of the *ortho*-methyl substituent in complex **3** slowing down hydrolysis. It is important to note that depending on the pH of the cell and the pK_a of the aqua adduct, the complex can be present in either the less reactive hydroxo or in its reactive aqua form (Table 5, Supporting Information, Figure S2).

Compounds **3A**, [(η^6-bip)Os(6-Me-pico)D_2O]$^+$, **4A**, [(η^6-bip)Os(4-Cl-pico)D_2O]$^+$, **5A**, [(η^6-bip)Os(4-CO_2H-pico)-D_2O]$^+$, and **6A**, [(η^6-bip)Os(4-Me-pico)D_2O]$^+$, have similar pK_a* values, ranging from 6.30 to 6.61 (Table 6). This shows that substituents on the picolinate chelating ligand have little effect on the acidity of the bound water. These values are significantly lower (ca. 1.5 units) than those for structurally similar Ru^{II} arene aqua complexes.[2,6] The pK_a* values of **3A**−**6A** (<7, Table 6) indicate that at physiological pH (7.4) almost all of **3A**−**6A** would be present in their less reactive hydroxo forms. Furthermore, the carboxylic acid substituent of compound **5** (pK_a* 2.5), would be present in its deprotonated form at physiological pH giving an overall negative charge on **5** (i.e., [(η^6-bip)Os(4-CO_2-pico)Cl]$^-$).

Interaction with Nucleobase Derivatives; 9-Ethyl Guanine (9EtG) and 9-Ethyl Adenine (9EtA). Nuclear DNA is believed to be a major target for transition metal-based anticancer complexes.[27] Osmium arene complexes, $[(\eta^6\text{-arene})Os(XY)Cl]^{n+}$, containing a neutral *N,N*-chelate (e.g., ethylenediamine) bind selectively to G nucleobases, and those containing an anionic *O,O*-chelate (e.g., acetylacetonate) have similar affinities for both G and A nucleobases.[2]

In this study, the interactions with nucleobase derivatives, 9-ethyl guanine (9EtG) and 9-ethyl adenine (9EtA) with compounds **1**−**6** in D_2O were investigated (Table 7, Figure 4). Compounds **4**−**6** bind significantly (60−100%) to both nucleobases. Compound **6** appears to bind more weakly to 9EtA which indicates a slightly weaker binding of **6** to adenine compared to guanine. Compound **5** shows exceptionally high nucleobase affinity with 100% nucleobase adduct formation for both 9EtG and 9EtA after 24 h. Compound **4** reacted more slowly with both nucleobases with equilibration reached after 72 h, while the other compounds reacted with the nucleobases within 24 h. (Table 7). Compounds **1**−**3** containing *ortho*-substituents, reacted significantly less with the model nucleobases (Figure 4), indicating weaker binding to G and A bases for these complexes. This weaker binding is most likely due to the steric hindrance caused by the *ortho*-substituents on the

picolinate ring. This is more evident for **3** compared to compound **6**, which both contain a methyl substituent displaying a similar electronic effect but with only **3** (*ortho*-Me) causing steric hindrance at Os. Compound **3** is significantly less reactive toward these nucleobases compared to compound **6** with about 50% less binding observed to both 9-ethyl guanine and 9-ethyl adenine after 24 h. ADF calculations confirm that the minimum energies of geometry-optimized structures of the nucleobase adducts of **6** are significantly lower than those found for its isomer complex **3**; **9EtG-6** was found to be 6.6 kcal/mol more stable than **9EtG-3**, and **9EtA-6** was 5.8 kcal/mol more stable than **9EtA-3**, indicating that the nucleobase adducts of complex **6** are thermodynamically more stable than those of complex **3**.

In contrast to compounds **3**−**6**, compound **1** formed no adduct with 9EtG but does, however, form adducts with 9EtA. Minimum energy structures of the 9EtA adduct with complex **1**, ([(η^6-bip)Os(6-Br-pico)(9EtA)], Supporting Information, Figure S5B), obtained from DFT calculations do indeed show hydrogen bonding between the NH_2 group of adenine and the carboxylate of the picolinate ligand, stabilizing this adduct. In contrast, the minimum energy structure of the 9EtG adduct, ([(η^6-bip)Os(6-Br-pico)(9EtG)]), shows a close contact between the bromide substituent and the guanine C6O which might explain the lack of reactivity of complex **1** with 9EtG (Supporting Information, Figure S5A). This argument can also be used to explain the same observed nucleobase specificity of complex **2**. Also, both compounds **1** and **2** form two adducts with 9EtA, a behavior which is not observed for any of the other osmium complexes **3**−**6** (Table 7).

Cytotoxicity. Compounds **1**−**3** and **5** were non-toxic toward colon HCT116, human lung A549, human ovarian A2780, and cisplatin resistant A2780cis cancer cell lines. Compounds **4** and **6**, however, exhibited promising toxicity, with IC_{50} values similar to those for cisplatin in the human ovarian A2780 and colon HCT116 cancer cell lines, and moderate cytotoxicity in the A549 cancer cell line with IC_{50} values about three times that of cisplatin. Interestingly, both compounds **4** and **6** overcome cisplatin resistance in the A2780cis cell line indicating that the mechanism of action of these osmium arene complexes is different from that of cisplatin (Table 8).

The steric bulk present around the metal center caused by the *ortho*-substituents in the picolinate compounds **1**−**3** accompanied by their reluctance to form nucleobase adducts may account for their cytotoxic inactivity. This is further supported by their reduced 9EtG and 9EtA binding, especially comparing complex **3** with complex **6** and the slower hydrolysis rates observed for compounds **1** and **3.** The cytotoxic inactivity of compound **5** might arise from poor cellular uptake as a result of the deprotonation of its *para*-substituent carboxyl group (pK_a* 2.5, Table 6), and overall negative charge. This hypothesis is supported by the observed activity of compound **7** which has an ester group in the *para* position in the human ovarian A2780 and A2780cis cancer cell lines (Table 8).

Conclusions

In this study, we have shown how steric and electronic effects of substituents on the *ortho*- and *para*-position of picolinate chelated to [(η^6-arene)$Os^{II}Cl]^+$ fragments can be used to control hydrolysis rates, extent of nucleobase (G and A) binding, and cancer cell cytotoxicity. Faster hydrolysis is observed with an electron-donating methyl group (compound **6**) and slower hydrolysis for the electron-withdrawing chloro and carboxyl groups (compounds **4** and **5**, respectively, see Table 3) in the *para*-position.

Of the 6 compounds tested, compounds **4** and **6** show promising activity in the human ovarian A2780 and human colon HCT116 cancer cell lines with similar IC_{50} values to those of cisplatin (see Table 8) and even overcome cisplatin resistance in the A2780cis cell line, indicating that the mechanism of action of these osmium arene complexes is different from that of cisplatin.

The cytotoxic inactivity of compounds **1**−**3** may be caused by the presence of sterically demanding *ortho*-substituents on the pyridine ring which hinder attack on the metal center. The effect of the steric hindrance is further demonstrated by their relatively slow hydrolysis rates and their reduced and weaker binding to guanine and adenine especially for complex **3** in comparison to complex **6** (Table 7, Figure 4), which differ only by having the methyl substituent at the *ortho*- and *para*-positions of the picolinate ring, respectively.

The cytotoxic inactivity of compound **5** might be caused by the deprotonation of its *para*-substituent carboxyl group (pK_a* 2.5), resulting in an overall negative charge (in its chloro form) in aqueous conditions hindering cellular uptake. Also, even if complex **5** is taken up into the cell and activated by hydrolysis to its neutral aqua form, the lack of a positive charge might hinder its attack on DNA (which is negatively charged). To investigate the influence of charge, the ethyl ester, compound **7**, was synthesized, and its cytotoxicity was determined in the A2780 and A2780cis cell lines. Its moderate cytotoxic activity (Table 8) suggests that the overall negative charge in complex **5** does indeed contribute to its inactivity.

This work shows that substituents on the picolinate backbone can have significant effects on the aqueous chemistry of osmium(II) compounds of the type [(η^6-bip)Os(YZ)(Cl)] allowing a great scope for design for this class of compounds. The synthetic route for compound **7** illustrates as well a new way of functionalizing osmium arene compounds which could be applied to a wide range of other osmium compounds. This study shows that we are able to introduce desirable features into these types of complexes to optimize their design as anticancer drugs.

Acknowledgment. We thank the EPSRC National Crystallography Service (Dr Peter Horton, University of Southampton) for collecting the diffraction data for complex **6**. We thank Dr. R. Deeth for advice on the use of ADF. We thank Dr M. Khan (Warwick University), Dr A.M. Pizarro (Warwick University), and Rhona Aird (General Hospital, Edinburgh) for help and advice on cell culture. This research was supported by Engineering and Physical Sciences Research

Council (EPSRC) and Warwick University. The authors also acknowledge that their participation in the EU COST Action D39 enabled them to exchange regularly the most recent ideas in the field of anticancer metallodrugs with several European colleagues.

Supporting Information Available: Time dependence for hydrolysis of **3**, **4**, and **5** (Figure S1), effect of various concentrations of Cl^- ion on the hydrolysis of **3** and **6** (Figure S2), ^1H NMR spectra of the pH titration of 6A and 5A (Figure S3), plots of the ^1H NMR chemical shifts of the coordinated arene ring protons versus pH* (Figure S4), and optimized geometries for the nucleobase adducts of **1**, **3**, and **6** (Figure S5). This material is available free of charge via the Internet at http://pubs.acs.org.

IC8020222